

# Neutralino Annihilation into a Photon and a $Z$ Boson

Piero Ullio\*

Department of Theoretical Physics, Uppsala University,  
Box 803, SE-751 08 Uppsala, Sweden  
and Department of Physics, Stockholm University,  
Box 6730, SE-113 85 Stockholm, Sweden

Lars Bergström†

Department of Physics, Stockholm University,  
Box 6730, SE-113 85 Stockholm, Sweden

October 24, 1997

## Abstract

A full one-loop calculation of neutralino  $S$ -wave annihilation into the  $Z\gamma$  final state is performed in the minimal supersymmetric extension of the Standard Model. This process, like the similar one with two photons in the final state, may be of importance for the indirect detection of supersymmetric dark matter through the very narrow  $\gamma$  ray line that would result from neutralino annihilations in the galactic halo.

We give the complete analytical formulas for this loop-induced process and treat the case of a pure Higgsino as a first application of our expressions. Predictions for the gamma line flux are given for the halo model which is of the form suggested by Kravtsov et al. and for the profile proposed by Navarro, Frenk and White.

For heavy neutralinos, the lines from  $2\gamma$  and  $Z\gamma$  would have indistinguishable energy in a realistic detector, making the fluxes add and facilitating discovery. For lighter neutralinos, the positions and relative strengths of the two lines would give valuable information on the nature of the supersymmetric dark matter particles.

---

\*piero@physto.se

†lbe@physto.se

# 1 Introduction

Although the lightest supersymmetric particle, generally assumed to be a neutralino, is an excellent dark matter candidate it is not easy to prove the hypothesis that the massive halo of the Milky Way is predominantly composed of such particles. Due to the weak interaction strength, direct detection of neutralino scattering requires detectors of a sensitivity which only recently has started to come close to that needed according to theoretical predictions.

In fact, even if there would appear a direct detection signal, it would most likely take a long time before it is established as a discovery due to the rather featureless recoil spectrum and the weak temporal modulations caused by the Earth's motion in the "wind" of neutralinos.

A similar lack of distinctive signature is plaguing indirect detection of antiprotons, positrons and continuum gamma emission from neutralino annihilation in the galactic halo. A better signature is provided by high-energy neutrinos from neutralino annihilation in the centre of the Sun or the Earth, but km<sup>2</sup>-scale neutrino detectors may be needed to scan a substantial portion of supersymmetric parameter space.\*

An excellent signature is given by a gamma ray line from neutralino annihilation into a two-body final state with at least one photon. Since the neutralinos annihilate with galactic velocities, i.e. non-relativistically, the photon in the process  $\tilde{\chi} + \tilde{\chi} \rightarrow \gamma + X^0$  (where  $\chi$  is the neutralino and  $X^0$  is a neutral particle) will be emitted with energy

$$E_\gamma = M_\chi - \frac{m_\chi^2}{4M_\chi}. \quad (1)$$

In a recent paper [2], we have performed a full one-loop calculation for the case  $X^0 = \gamma$ , i.e.  $\tilde{\chi}_1^0 + \tilde{\chi}_1^0 \rightarrow \gamma + \gamma$ , where  $\tilde{\chi}_1^0$  is the lightest of the four neutralinos in MSSM, the minimal supersymmetric extension of the Standard Model of particle physics. There it was shown that the  $\gamma\gamma$  process can be at least an order of magnitude larger than earlier simpler estimates indicated, especially for the very heavy, pure higgsino case (however, even this larger rate is several orders of magnitude below that needed to explain the possible structure in the multi-TeV gamma spectrum recently reported in [3], unless the halo dark matter is very clumpy [2]).

As there soon will exist new gamma-ray detectors, both space-borne and on Earth, with an order of magnitude larger detection area than that of existing ones, it is of importance to investigate other neutralino annihilation channels which give a nearly monoenergetic  $\gamma$ . In the MSSM, the only other such final state is  $Z^0\gamma$  [4]. Note that since the annihilation in the halo takes place in the  $S$  partial wave, helicity conservation forbids the  $H_i^0\gamma$  final state with  $i = 1, 2, 3$  representing the three neutral Higgs bosons. There may be non-perturbative final states, such as  $V\gamma$  with  $V$  a vector meson made from a  $q\bar{q}$  pair, but these generally have a very small branching ratio [5, 6].

As we will see in the case of a pure higgsino, the  $Z^0\gamma$  and  $\gamma\gamma$  cross sections are of about equal magnitude. This gives an interesting way to verify the gamma ray detection of neutralino dark matter: there should be two lines with energy ratio

$$\frac{E_{1\gamma}}{E_{2\gamma}} = 1 - \frac{m_Z^2}{4M_\chi^2}. \quad (2)$$

---

\*For a thorough discussion of the various detection methods, see [1].

For a heavy higgsino, the two lines would hardly be resolvable resulting in a further increase of the line strength compared to the results of [2]. For a lower neutralino mass (below a few hundred GeV) the two lines would be resolved. The relative strengths of the two lines could give a handle on the composition of the neutralino. This comes about because despite the fact that the two processes are closely related there are some differences (e.g. the non-diagonal couplings of  $Z^0$  to charginos and squarks) which depend on composition. We leave the detailed investigation of this for future work, however.

## 2 Cross section

The process of neutralino annihilation into a photon and a  $Z^0$  boson

$$\tilde{\chi}_1^0 + \tilde{\chi}_1^0 \rightarrow \gamma + Z^0 \quad (3)$$

was briefly discussed in [4] but is examined here for the first time in a full one-loop calculation. We focus on the case of massive non-relativistic particles in the initial state, as this is the appropriate limit for neutralinos annihilating in the galactic halo (the predicted value of the velocity for dark matter particles in the halo is of the order of  $10^{-3} c$ ). The outgoing photons are nearly monochromatic, with energy

$$E_\gamma = M_\chi - \frac{m_Z^2}{4M_\chi}. \quad (4)$$

The steps we follow to compute the cross section are essentially the same as those described for the  $2\gamma$  case. As the P wave is highly suppressed, it is a very good approximation to assume that the neutralino pair is in a  $^1S_0$  state and to calculate the amplitude using the corresponding projector [7]. We notice that it is convenient to choose the non-linear gauge introduced in Ref [8] which has the peculiarity of having a vanishing coupling for the  $W^\pm G^\mp \gamma$  vertex ( $G^\mp$  is the unphysical Higgs or charged Goldstone boson). We reduce in this way the number of diagrams involving  $W^+$  and  $G^+$  loops. The diagrams giving a non-vanishing contribution to the cross section at the one loop level are shown in Figs. 1-4. Note that for a generic supersymmetric model the vertices  $Z^0 \tilde{f}_i \tilde{f}_j$  and  $Z^0 \chi_i^+ \chi_j^+$  are non diagonal respectively in the sfermion and the chargino mass eigenstates.

The computation of the loop diagrams is greatly simplified after realising that the four-point functions which arise from box diagrams can be rewritten as linear combinations of three-point functions. This procedure was already exploited in [2] and can be applied regardless of the final state, because the particles in the initial state, being identical particles at rest, have equal four-momenta. It is easy to verify that in this case it is possible to find a linear combination of three or four factors in the denominator of each four-point function which is independent of the momentum flowing in the loop and formally reduce the calculation to integrals of three-point functions.

We keep, where possible, the notation introduced in Ref. [2]. The amplitude of the process is factorized as

$$\mathcal{A} = \frac{e}{2\sqrt{2}\pi^2} \epsilon(\epsilon_1, \epsilon_2, k_1, k_2) \tilde{\mathcal{A}} \quad (5)$$

where  $\epsilon_1$  and  $k_1$  are the polarization tensor and the momentum of the photon in the final state, whereas  $\epsilon_2$  and  $k_2$  refer to the polarization tensor and the momentum of the  $Z^0$ . The cross section multiplied by  $v$ , the relative velocity of the neutralino pair, is given in terms of  $\tilde{\mathcal{A}}$  by the formula

$$v\sigma_{Z\gamma} = \frac{\alpha}{32\pi^4} \frac{(M_\chi^2 - m_Z^2/4)^3}{M_\chi^4} \left| \tilde{\mathcal{A}} \right|^2. \quad (6)$$

We have identified four classes of diagrams. The total amplitude is given as:

$$\tilde{\mathcal{A}} = \tilde{\mathcal{A}}_{f\bar{f}} + \tilde{\mathcal{A}}_{H^+} + \tilde{\mathcal{A}}_W + \tilde{\mathcal{A}}_G.$$

For each contribution we have separated real and imaginary parts. The results are not as compact as those obtained for the process of neutralino annihilation into two photons. This is due mainly to the presence in each class of diagrams of four mass parameters. The complexity of the calculation, and the many parameters entering the supersymmetric models means that it may be difficult to check our results numerically in an independent calculation. Therefore, we want to give all the analytical expressions despite the rather lengthy formulas. We have, however, chosen a notation that facilitates a comparison with the previous  $2\gamma$  results [2] in the limit when  $M_Z \rightarrow 0$ , and only diagonal terms are kept in the  $Z^0 \tilde{f}_i \tilde{f}_j$  and  $Z^0 \chi_i^+ \chi_j^+$  vertices.

### 1) Contribution of the fermion-sfermion loop diagrams.

This class of diagrams is shown in Fig. 1. The sum over  $f$  includes the quarks and the charged leptons, the sum over  $\tilde{f}_i$  and  $\tilde{f}_j$  the corresponding sfermion mass eigenstates.

$$\begin{aligned} Re \tilde{\mathcal{A}}_{f\bar{f}} = & \sum_f \frac{c_f \cdot e_f}{M_\chi^2 - m_Z^2/4} \left\{ \sum_{\tilde{f}_i} \left[ E_1 I_1^3(a, b, c/4) + E_2 \tilde{I}_2^3(a, b, c/4) \right. \right. \\ & + E_1 I_3^3(a, b, c/4) + (E_1 + E_3 + E_4) \tilde{I}_3^3(a, b, c/4) - \frac{S_{f\bar{f}}^b}{4} I_4^1(a, b, c) \left. \right] \\ & + \sum_{\tilde{f}_i \tilde{f}_j} \left[ (E_5 + E_6 + E_7) \tilde{I}_{2;1}^4(a, b, d, c/4) + (E_5 + E_6 - E_7) \tilde{I}_{2;2}^4(a, b, d, c/4) \right. \\ & \left. + E_8 I_3^3(a, b, c/4) + E_8 I_3^4(a, b, d, c/4) + \frac{S_{f\bar{f}}^a}{4} I_4^2(a, b, d, c) \right] \left. \right\} \\ & + \sum_f \frac{c_f \cdot e_f}{M_\chi^2 - m_Z^2/4} E_9 I_1^3(a, b, c/4) \end{aligned} \quad (7)$$

$$\begin{aligned} Im \tilde{\mathcal{A}}_{f\bar{f}} = & \pi \frac{c_f \cdot e_f}{M_\chi^2 - m_Z^2/4} \left\{ - \sum_f \left( \sum_{\tilde{f}_i} E_1 + E_9 \right) J_1(a, b) \theta(1 - m_f^2/M_\chi^2) \right. \\ & + \sum_f \left[ \left( \sum_{\tilde{f}_i} E_1 + E_9 \right) J_2(b, c) + \sum_{\tilde{f}_i} \left( (E_1 + E_3 + E_4) J_3(a, b, c) \right. \right. \end{aligned}$$

$$\left. + \frac{c}{8} \frac{\sqrt{1-4b/c} S_{f\bar{f}}^b}{a-c/4} \right] \theta(1-4m_f^2/m_Z^2) \} \quad (8)$$

$e_f$  is the charge of the fermion in units of the electron charge ( $-e$ ),  $c_f$  is the color factor equal to 3 for quarks and to 1 for leptons. The functions  $I$  and  $\bar{I}$  which appear in the real part arise from the loop integrations and the  $J$  functions are the corresponding contributions in the imaginary part; their explicit form is given in Appendix A. The coefficients  $E$  are listed below:

$$\begin{aligned} E_1 &= -\frac{b(S_{f\bar{f}}^b + S_{f\bar{f}}^c) + 2\sqrt{ab}D_{f\bar{f}}}{4(1+a-b)} \\ E_2 &= -\frac{1}{4} \frac{S_{f\bar{f}}^b}{1-b+c/4} \\ E_3 &= \frac{1}{4} \frac{(b-c/4)S_{f\bar{f}}^b}{1-b+c/4} \\ E_4 &= -\frac{c}{16} \frac{(1-b+c/4)S_{f\bar{f}}^b}{(a-c/4)^2} \\ E_5 &= -\frac{1}{8} \frac{(1/2+d/2-c/4)S_{f\bar{f}}^a}{1/2+d/2-b-c/4} \\ E_6 &= -\frac{c}{32} \frac{(1/2+d/2-b-c/4)S_{f\bar{f}}^a}{(a-c/4)^2} \\ E_7 &= \frac{1}{16} \frac{(1-d)S_{f\bar{f}}^a}{a-c/4} \\ E_8 &= \frac{1}{8} \frac{bS_{f\bar{f}}^a}{1/2+d/2-b-c/4} \\ E_9 &= \frac{m_f^2 G_{Zf}}{4m_Z^2} - \frac{m_f M_\chi G_{H_3^0 f}}{4(4M_\chi^2 - m_{H_3^0}^2)} \end{aligned}$$

where we have defined:

$$\begin{aligned} a &= \frac{M_{\chi_1^0}^2}{M_{\bar{f}_i}^2} & b &= \frac{m_f^2}{M_{\bar{f}_i}^2} \\ c &= \frac{m_Z^2}{M_{\bar{f}_i}^2} & d &= \frac{M_{\bar{f}_j}^2}{M_{\bar{f}_i}^2} \end{aligned}$$

$$\begin{aligned} D_{f\bar{f}} &= \frac{1}{4} \left( g_{\bar{f}_i f_1}^L g_{\bar{f}_i f_1}^{R*} + g_{\bar{f}_i f_1}^R g_{\bar{f}_i f_1}^{L*} \right) \cdot (g_{Zff}^L + g_{Zff}^R) \\ S_{f\bar{f}}^a &= \frac{g_{\bar{f}_i \bar{f}_j}}{2} \left( g_{\bar{f}_j f_1}^L g_{\bar{f}_i f_1}^{L*} + g_{\bar{f}_j f_1}^R g_{\bar{f}_i f_1}^{R*} \right) \end{aligned}$$

$$\begin{aligned}
S_{f\bar{f}}^b &= \frac{1}{2} \left( g_{\bar{f}_i f_1}^L g_{\bar{f}_i f_1}^{L*} g_{Zff}^R + g_{\bar{f}_i f_1}^R g_{\bar{f}_i f_1}^{R*} g_{Zff}^L \right) \\
S_{f\bar{f}}^c &= \frac{1}{2} \left( g_{\bar{f}_i f_1}^L g_{\bar{f}_i f_1}^{L*} g_{Zff}^L + g_{\bar{f}_i f_1}^R g_{\bar{f}_i f_1}^{R*} g_{Zff}^R \right) \\
G_{Zf} &= \frac{1}{2} \left( g_{Z11}^L - g_{Z11}^R \right) \left( g_{Zff}^L{}^2 - g_{Zff}^R{}^2 \right) \\
G_{H_3^0 f} &= \frac{1}{2} \left( g_{H_3^0 11}^L - g_{H_3^0 11}^R \right) \left( g_{H_3^0 ff}^L - g_{H_3^0 ff}^R \right) \left( g_{Zff}^L + g_{Zff}^R \right)
\end{aligned}$$

The index 1 is referred to  $\tilde{\chi}_1^0$ .

## 2) Contribution of the chargino-Higgs boson loop diagrams.

This class of diagrams is shown in Fig. 2. The sums over  $\chi_i^\pm$  and  $\chi_j^\pm$  involves the two chargino mass eigenstates.

$$\begin{aligned}
Re \tilde{\mathcal{A}}_{H^+} &= \sum_{\chi_i^+} \frac{1}{M_\chi^2 - m_Z^2/4} \left\{ \left[ F_1 I_2^3(a, b, c/4) + (F_2 + F_3) \tilde{I}_3^3(a, b, c/4) \right. \right. \\
&\quad \left. \left. + \frac{S_{\chi H}^a}{4} I_4^1(a, b, c) \right] + \sum_{\chi_j^+} \left[ (F_4 + F_{10}) I_1^4(a, d, 1, c/4) \right. \right. \\
&\quad \left. \left. + (F_5 + F_{11}) I_1^4(a, 1, d, c/4) + F_4 I_2^3(a, b, c/4) \right. \right. \\
&\quad \left. \left. + F_5 I_2^4(a, b, d, c/4) + (F_5 + F_6 + F_7 + F_8) \tilde{I}_{2;1}^4(a, b, d, c/4) \right. \right. \\
&\quad \left. \left. + (F_4 - F_6 + F_7 + F_8) \tilde{I}_{2;2}^4(a, b, d, c/4) + F_9 I_3^3(a, b, c/4) \right. \right. \\
&\quad \left. \left. + F_9 I_3^4(a, b, d, c/4) - \frac{S_{\chi H}^b}{4} I_4^2(a, b, d, c) \right] \right\} \quad (9)
\end{aligned}$$

The coefficients F are listed below:

$$\begin{aligned}
F_1 &= -\frac{1}{4} \frac{S_{\chi H}^a}{1-b+c/4} \\
F_2 &= \frac{1}{4} \frac{(b-c/4) S_{\chi H}^a}{1-b+c/4} \\
F_3 &= \frac{c}{16} \frac{(1-b+c/4) S_{\chi H}^a}{(a-c/4)^2} \\
F_4 &= \frac{1}{8} \frac{2\sqrt{a} D_{\chi H}^b + \sqrt{d} S_{\chi H}^c + S_{\chi H}^b}{1/2 + d/2 - a - b} \\
F_5 &= \frac{1}{8} \frac{2\sqrt{a}\sqrt{d} D_{\chi H}^c + \sqrt{d} S_{\chi H}^c + d S_{\chi H}^b}{1/2 + d/2 - a - b} \\
F_6 &= -\frac{1}{8} \frac{\sqrt{a} D_{\chi H}^b - \sqrt{a}\sqrt{d} D_{\chi H}^c}{a-c/4} - \frac{1}{16} \frac{(1-d) S_{\chi H}^b}{a-c/4} \\
F_7 &= \frac{c}{32} \frac{(1/2 + d/2 - b - c/4) S_{\chi H}^b}{(a-c/4)^2}
\end{aligned}$$

$$\begin{aligned}
F_8 &= -\frac{1}{8} \frac{(1/2 + d/2 - c/4) S_{\chi H}^b}{(1/2 + d/2 - b - c/4)} \\
F_9 &= \frac{1}{8} \frac{b S_{\chi H}^b}{(1/2 + d/2 - b - c/4)} \\
F_{10} &= \frac{1}{16} \frac{\sqrt{d} D_Z + S_Z}{c} + \frac{1}{8} \frac{\sqrt{a} S_{H^0}}{4a - m_{H_3^0}^2/M_{\chi_i^+}^2} \\
F_{11} &= \frac{1}{16} \frac{\sqrt{d} D_Z + d S_Z}{c} + \frac{1}{8} \frac{\sqrt{a} \sqrt{d} D_{H^0}}{4a - m_{H_3^0}^2/M_{\chi_i^+}^2}
\end{aligned}$$

and we have defined:

$$\begin{aligned}
a &= \frac{M_{\chi_1^0}^2}{M_{\chi_i^+}^2} & b &= \frac{m_{H^+}^2}{M_{\chi_i^+}^2} \\
c &= \frac{m_Z^2}{M_{\chi_i^+}^2} & d &= \frac{M_{\chi_j^+}^2}{M_{\chi_i^+}^2}
\end{aligned}$$

$$\begin{aligned}
S_{\chi H}^a &= \frac{g_{ZH^+H^+}}{2} (g_{H^+1i}^L g_{H^+1i}^{L*} + g_{H^+1i}^R g_{H^+1i}^{R*}) \\
S_{\chi H}^b &= \frac{1}{2} (g_{H^+1j}^L g_{H^+1i}^{L*} g_{Zji}^L + g_{H^+1j}^R g_{H^+1i}^{R*} g_{Zji}^R) \\
D_{\chi H}^b &= \frac{1}{2} (g_{H^+1j}^L g_{H^+1i}^{R*} g_{Zji}^L + g_{H^+1j}^R g_{H^+1i}^{L*} g_{Zji}^R) \\
S_{\chi H}^c &= \frac{1}{2} (g_{H^+1j}^L g_{H^+1i}^{L*} g_{Zji}^R + g_{H^+1j}^R g_{H^+1i}^{R*} g_{Zji}^L) \\
D_{\chi H}^c &= \frac{1}{2} (g_{H^+1j}^L g_{H^+1i}^{R*} g_{Zji}^R + g_{H^+1j}^R g_{H^+1i}^{L*} g_{Zji}^L) \\
S_Z &= (g_{Z11}^L - g_{Z11}^R) (g_{Zij}^L g_{Zji}^L - g_{Zij}^R g_{Zji}^R) \\
D_Z &= (g_{Z11}^L - g_{Z11}^R) (g_{Zij}^L g_{Zji}^R - g_{Zij}^R g_{Zji}^L) \\
S_{H^0} &= (g_{H_3^0 11}^R - g_{H_3^0 11}^L) (g_{H_3^0 ij}^L g_{Zji}^L - g_{H_3^0 ij}^R g_{Zji}^R) \\
D_{H^0} &= (g_{H_3^0 11}^R - g_{H_3^0 11}^L) (g_{H_3^0 ij}^L g_{Zji}^R - g_{H_3^0 ij}^R g_{Zji}^L)
\end{aligned}$$

where the indices  $i$  and  $j$  are referred to  $\tilde{\chi}_i^+$  and  $\tilde{\chi}_j^+$

### 3) Contribution of the chargino-W boson loop diagrams.

This class of diagrams is shown in Fig. 3.

$$Re \tilde{A}_W = \sum_{\chi_i^+} \frac{1}{M_{\chi}^2 - m_Z^2/4} \left\{ \left[ G_1 I_1^3(a, b, c/4) + G_2 I_2^3(a, b, c/4) \right] \right.$$

$$\begin{aligned}
& + G_3 I_3^3(a, b, c/4) + (G_3 + G_4 + G_9) \tilde{I}_3^3(a, b, c/4) - \frac{S_{\chi W}^a}{2} I_4^1(a, b, c) \Big] \\
& + \sum_{x_j^+} \left[ G_5 I_1^4(a, d, 1, c/4) + G_6 I_1^4(a, 1, d, c/4) + G_5 I_2^3(a, b, c/4) \right. \\
& \quad + G_6 I_2^4(a, b, d, c/4) + (G_6 + G_7 + G_{10} + G_{11}) \tilde{I}_{2;1}^4(a, b, d, c/4) \\
& \quad + (G_5 + G_7 + G_{10} - G_{11}) \tilde{I}_{2;2}^4(a, b, d, c/4) + G_8 I_3^3(a, b, c/4) \\
& \quad \left. + G_8 I_3^4(a, b, d, c/4) - \frac{S_{\chi W}^b}{2} I_4^2(a, b, d, c) \right] \Big\} \tag{10}
\end{aligned}$$

$$Im \tilde{A}_W = -\pi \sum_{x_i^+} \frac{1}{M_\chi^2 - m_Z^2/4} G_1 J_1(a, b) \theta(1 - m_W^2 / M_\chi^2) \tag{11}$$

The coefficients G are given by:

$$\begin{aligned}
G_1 &= 2 \frac{(a-b) S_{\chi W}^a}{1+a-b} \\
G_2 &= -\frac{1}{2} \frac{3 S_{\chi W}^a - 4\sqrt{a} D_{\chi W}^a}{1-b+c/4} \\
G_3 &= -\frac{(1-a+b) S_{\chi W}^a}{1+a-b} \\
G_4 &= \frac{1}{2} \frac{(2+b-c/4) S_{\chi W}^a - 4\sqrt{a} D_{\chi W}^a}{1-b+c/4} \\
G_5 &= \frac{1}{2} \frac{2\sqrt{a} D_{\chi W}^b - (\sqrt{d}/2 + 1/2) S_{\chi W}^b}{1/2 + d/2 - a - b} \\
G_6 &= \frac{1}{2} \frac{2\sqrt{a}\sqrt{d} D_{\chi W}^b - (\sqrt{d}/2 + d/2) S_{\chi W}^b}{1/2 + d/2 - a - b} \\
G_7 &= -\frac{1}{2} \frac{\sqrt{a}(\sqrt{d}+1) D_{\chi W}^b - (\sqrt{d} + d/4 + 1/4 + c/8) S_{\chi W}^b}{1/2 + d/2 - b - c/4} \\
G_8 &= \frac{1}{2} \frac{\sqrt{a}(\sqrt{d}+1) D_{\chi W}^b - (\sqrt{d} + b/2 + c/4) S_{\chi W}^b}{1/2 + d/2 - b - c/4} \\
G_9 &= -\frac{c}{8} \frac{(1-b+c/4) S_{\chi W}^a}{(a-c/4)^2} \\
G_{10} &= \frac{c}{16} \frac{(1/2 + d/2 - b - c/4) S_{\chi W}^b}{(a-c/4)^2} \\
G_{11} &= -\frac{1}{8} \frac{(1-d) S_{\chi W}^b}{(a-c/4)}
\end{aligned}$$



where we have defined:

$$a = \frac{M_{\chi_1^0}^2}{M_{\chi_i^+}^2} \quad b = \frac{m_W^2}{M_{\chi_i^+}^2}$$

$$c = \frac{m_Z^2}{M_{\chi_i^+}^2} \quad d = \frac{M_{\chi_j^+}^2}{M_{\chi_i^+}^2}$$

$$S_{\chi W}^a = \frac{g \cos \theta_W}{2} (g_{W1i}^L g_{W1i}^{L*} + g_{W1i}^R g_{W1i}^{R*})$$

$$D_{\chi W}^a = \frac{g \cos \theta_W}{2} (g_{W1i}^L g_{W1i}^{R*} + g_{W1i}^R g_{W1i}^{L*})$$

$$S_{\chi W}^b = \frac{1}{4} (g_{W1j}^L g_{W1i}^{L*} + g_{W1j}^R g_{W1i}^{R*}) \cdot (g_{Zji}^L + g_{Zji}^R)$$

$$D_{\chi W}^b = \frac{1}{4} (g_{W1j}^L g_{W1i}^{R*} + g_{W1j}^R g_{W1i}^{L*}) \cdot (g_{Zji}^L + g_{Zji}^R)$$

#### 4) Contribution of the chargino-unphysical Higgs loop diagrams.

This class of diagrams is shown in Fig. 4.

$$Re \tilde{A}_G = \sum_{\chi_i^+} \frac{1}{M_{\chi_i^+}^2 - m_Z^2/4} \left\{ \left[ (H_1 + H_{10}) I_2^3(a, b, c/4) + (H_2 + H_3 - H_{10}) \tilde{I}_3^3(a, b, c/4) \right. \right.$$

$$+ \left. \frac{S_{\chi G}^a}{4} I_4^1(a, b, c) \right] + \sum_{\chi_j^+} \left[ H_4 I_1^4(a, d, 1, c/4) + H_5 I_1^4(a, 1, d, c/4) \right.$$

$$+ H_4 I_2^3(a, b, c/4) + H_5 I_2^4(a, b, d, c/4) + (H_5 + H_6 + H_7 + H_8) \tilde{I}_{2;1}^4(a, b, d, c/4)$$

$$+ (H_4 - H_6 + H_7 + H_8) \tilde{I}_{2;2}^4(a, b, d, c/4) + H_9 I_3^3(a, b, c/4)$$

$$\left. \left. + H_9 I_3^4(a, b, d, c/4) - \frac{S_{\chi G}^b}{4} I_4^2(a, b, d, c) \right] \right\} \quad (12)$$

For  $i \in \{1..9\}$  the coefficient  $H_i$  is obtained from the corresponding  $F_i$  substituting  $S_{\chi H}^p$  and  $D_{\chi H}^p$  respectively with  $S_{\chi G}^p$  and  $D_{\chi G}^p$ .  $H_{10}$  is given by:

$$H_{10} = -\frac{\sqrt{c}}{4} \frac{S_{\chi G}^d + D_{\chi G}^d}{1 - b + c/4}$$

a,b,c,d are defined as in the case of the chargino-W boson contribution and we have introduced:

$$S_{\chi G}^a = \frac{g Z G G}{2} (g_{G1i}^L g_{G1i}^{L*} + g_{G1i}^R g_{G1i}^{R*})$$

$$\begin{aligned}
S_{\chi G}^b &= \frac{1}{2} (g_{G1j}^L g_{G1i}^{L*} g_{Zji}^L + g_{G1j}^R g_{G1i}^{R*} g_{Zji}^R) \\
D_{\chi G}^b &= \frac{1}{2} (g_{G1j}^L g_{G1i}^{R*} g_{Zji}^L + g_{G1j}^R g_{G1i}^{L*} g_{Zji}^R) \\
S_{\chi G}^c &= \frac{1}{2} (g_{G1j}^L g_{G1i}^{L*} g_{Zji}^R + g_{G1j}^R g_{G1i}^{R*} g_{Zji}^L) \\
D_{\chi G}^c &= \frac{1}{2} (g_{G1j}^L g_{G1i}^{R*} g_{Zji}^R + g_{G1j}^R g_{G1i}^{L*} g_{Zji}^L) \\
S_{\chi G}^d &= \frac{g}{2} (g_{W1i}^L g_{G1i}^{L*} + g_{W1i}^R g_{G1i}^{R*}) \\
D_{\chi G}^d &= \frac{g}{2} (g_{G1i}^L g_{W1i}^{R*} + g_{G1i}^R g_{W1i}^{L*})
\end{aligned}$$

The coupling constants for left and right chiral states,  $g^L$  and  $g^R$ , are written in the conventions adopted in the PhD Thesis of Edsjö [9]; all of them are defined therein but  $g_{G1i}^L$  and  $g_{G1i}^R$  which are given in [2] and

$$g_{ZGG} = \bar{g}_{ZH^+H^+}$$

Note that a sign factor is implied wherever a square root of a mass parameter appears. For instance, in the third class of diagrams

$$\sqrt{a} = \text{sign}(M_{\chi_1^0}/M_{\chi_i^+}) \cdot \sqrt{M_{\chi_1^0}^2/M_{\chi_i^+}^2} \quad (13)$$

In this way we take into account the fact that, if the convention of real neutralino and chargino mixing matrices is adopted, the mass eigenvalues can be either positive or negative.

We have checked the result of the imaginary part applying the Cutkosky rules. These provide a general scheme to extract the imaginary part which is the contribution to the amplitude deriving from physical intermediate states in the loop diagrams (for a review see for instance Ref [10]). It is sufficient to examine if in each diagram it is possible to identify two separate processes that are both kinematically allowed.

### 3 Pure Higgsino limit

The calculation of the annihilation rate involves many subtleties. Although all integral expressions given here are convergent, they often individually have large values with severe cancellations between different terms. We have checked that our results reproduce the corresponding  $2\gamma$  ones in the limit  $M_Z \rightarrow 0$ .

As there has recently been some interest in the TeV region due to a claim in the literature for a possible structure in the gamma ray energy spectrum [3], we give as a first application of our results a treatment of the pure higgsino case<sup>†</sup>, leaving a more complete phenomenological analysis for a future work.

We now present the results for a pure higgsino initial state. Apart from small contributions from the fermion diagrams, only the diagrams in Fig. 3 give an important contribution. The

<sup>†</sup>The demand of not overclosing the Universe generally means that such a heavy neutralino has to have a very large higgsino fraction [11].

mass of the heaviest chargino goes to infinity, so the indices  $i$  and  $j$  refer to the lightest chargino. The latter is nearly degenerate in mass with  $\chi_1^0$ . We find a compact expression which can be easily implemented numerically.

$$\begin{aligned}
Re \tilde{\mathcal{A}} = & \frac{1}{M_\chi^2 - m_Z^2/4} \left[ C_1 I_1^3(a, b, c/4) + 2 C_5 I_1^3(a, 1, c/4) \right. \\
& + (C_2 + 2 C_5) I_2^3(a, b, c/4) + 2 (C_5 + C_7 + C_{10}) \tilde{I}_2^3(a, b, c/4) \\
& + (C_3 + 2 C_8) I_3^3(a, b, c/4) + (C_3 + C_4 + C_9) \tilde{I}_3^3(a, b, c/4) \\
& \left. - \frac{S_{\chi W}^a}{2} I_4^1(a, b, c) - \frac{S_{\chi W}^b}{2} I_4^2(a, b, 1, c) \right] \quad (14)
\end{aligned}$$

$$Im \tilde{\mathcal{A}} = -\pi \frac{1}{M_\chi^2 - m_Z^2/4} C_1 J_1(a, b) \theta(1 - m_W^2 / M_\chi^2) \quad (15)$$

The coefficients  $C_i$  are obtained from the corresponding  $G_i$  with  $d=1$ . The degeneration in mass between the neutralino and lightest chargino gives  $a \simeq 1$ , while the couplings are:

$$\begin{aligned}
S_{\chi W}^a = D_{\chi W}^a &= \frac{g^3 \cos \theta_W}{4} \\
S_{\chi W}^b = D_{\chi W}^b &= \frac{g^3}{4 \cos \theta_W} \left( -\frac{1}{2} + \sin^2 \theta_W \right)
\end{aligned}$$

In Fig. 5, we show the values of  $v\sigma_{Z\gamma}$  obtained from these expressions, as a function of higgsino mass. As can be seen, the maximum value is around  $3.6 \cdot 10^{-28} \text{ cm}^3\text{s}^{-1}$  for a higgsino mass around 140 GeV. For higher masses, the value of  $v\sigma_{Z\gamma}$  reaches a plateau of around  $0.6 \cdot 10^{-28} \text{ cm}^3\text{s}^{-1}$ . This interesting effect of a non-diminishing cross section with higgsino mass (which is due to a contribution to the real part of the amplitude coming from diagrams 3e and 3f) was found also for the  $2\gamma$  final state in the corresponding limit, which gave a value of  $1 \cdot 10^{-28} \text{ cm}^3\text{s}^{-1}$  [2]. In the same Figure, the contribution from the imaginary part is also shown. This drops quite fast for the highest masses, and constitutes a unitarity lower bound on the cross section which agrees with the one found in [4].

## 4 Halo models

An uncertain element in the calculation of the absolute gamma line flux from neutralino annihilation in the galactic halo is the detailed dark matter density distribution. Since the integration along the line of sight involves the square of the density, any density enhancement may affect the predicted flux appreciably.

Available observational data give only very poor constraints on the mass distribution within the Milky Way [12]. Assuming that dark matter profiles are of a universal functional form, we will examine two profiles derived with N-body simulations of hierarchical clustering in

cold dark matter cosmologies and fitted to a sample of dark matter dominated dwarf and low-surface brightness galaxies. We consider among the general profile family

$$\rho(r) \propto \frac{1}{(r/a)^\gamma [1 + (r/a)^\alpha]^{(\beta-\gamma)/\alpha}}, \quad (16)$$

the Kravtsov et al. profile [13], defined by  $(\alpha, \beta, \gamma) = (2, 3, 0.2)$  with a very mild singularity at the galactic centre, and the Navarro et al. profile [14], which has  $(\alpha, \beta, \gamma) = (1, 3, 1)$ . There are models [15] which have a more singular behaviour near the galactic centre, and which would give enormously enhanced rate in that direction. However, there is observational evidence against such singularities from cluster gravitational lensing and the rotation curves of dwarf spiral galaxies [16]. On the other hand, the discrepancy between the  $1/r$  central cusp of the Navarro et al. profile and the experimental data from the dwarf spheroidal DDO 154 has been explained in Ref. [17] assuming an additional component of dark baryons.

We fix the normalization of the two profiles assuming that the dark matter density at our galactocentric distance,  $R \simeq 8.5$  kpc, is  $\rho_0 \simeq 0.3 \text{ GeV/cm}^3$ , and we choose for the Navarro et al. profile  $a \simeq 25$  kpc (appropriate value for the Milky Way in an  $\Omega = 1$  cosmology [18]), while for the Kravtsov et al. we fix  $a \simeq 11$  kpc. We consider the profiles valid up to the capture radius of the black hole at the galactic centre ( $\sim 0.01$  pc for a mass of Sgr A\*  $M \simeq 10^6 M_\odot$ ).

The gamma ray flux from the  $Z\gamma$  process is given by

$$\begin{aligned} \Phi_\gamma(\psi) &= \frac{v\sigma_{Z\gamma}}{4\pi M_\chi^2} \int_{line\ of\ sight} \rho^2(l) dl(\psi) \\ &\simeq 1.87 \cdot 10^{-11} \left( \frac{v\sigma_{Z\gamma}}{10^{-29} \text{ cm}^3\text{s}^{-1}} \right) \left( \frac{10 \text{ GeV}}{M_\chi} \right)^2 \left( \frac{R}{8.5 \text{ kpc}} \right) \\ &\quad \cdot \left( \frac{\rho_0}{0.3 \text{ GeV/cm}^3} \right)^2 J(\psi) \text{ cm}^{-2}\text{s}^{-1}\text{sr}^{-1} \end{aligned} \quad (17)$$

where  $\psi$  is the angle between the direction of the galactic centre and that of observation and  $J(\psi)$  is a dimensionless function defined as

$$J(\psi) = \frac{1}{R \rho_0^2} \int_{line\ of\ sight} \rho^2(l) dl(\psi). \quad (18)$$

We have computed the function  $J(\psi)$  numerically and the result for the two halo models considered are given in Fig. 6. As can be seen, for angles larger than 60 degrees the two curves nearly coincide and this is true even if we vary the parameters around the chosen values. Towards the galactic centre the Navarro et al. profile gives a huge enhancement of  $J$ ; these values should be compared to the value 5.7, which is the maximal value (in the  $\psi = 0$  direction) of the corresponding function for a halo described by an isothermal sphere,  $(\alpha, \beta, \gamma) = (2, 2, 0)$ , with  $a = R$  [19]. For the Kravtsov et al. profile, the maximal value is  $J(\sim 0) \simeq 10$ .

We are now in the position of being able to give a firm prediction for the total line flux of  $\gamma$  rays for TeV-scale higgsinos. Since any presently conceivable detector will have an energy resolution not better than one per cent or so, one has to add the contributions from the  $2\gamma$

annihilation calculated in [2] and the  $Z\gamma$  process calculated here for the first time. With the Kravtsov et al. density profile, the flux in the direction of the galactic centre is given by

$$\begin{aligned}\Phi_\gamma^{tot}(0) &\simeq 1.8 \cdot 10^{-14} \left( \frac{2v\sigma_{2\gamma} + v\sigma_{Z\gamma}}{10^{-29} \text{ cm}^3\text{s}^{-1}} \right) \left( \frac{1 \text{ TeV}}{M_\chi} \right)^2 \text{ cm}^{-2}\text{s}^{-1}\text{sr}^{-1} \\ &\simeq 4 \cdot 10^{-13} \left( \frac{1 \text{ TeV}}{M_\chi} \right)^2 \text{ cm}^{-2}\text{s}^{-1}\text{sr}^{-1}.\end{aligned}\tag{19}$$

Although this flux is much higher than previous estimates have indicated, it is still far from what is needed to explain the structure claimed in [3].

The new generation of large area air Cherenkov telescopes may have a sensitivity that comes close to the flux predicted in Eq. (19). Moreover, exploiting their very small angular acceptance ( $\sim 10^{-3}\text{sr}$ ), they will be able to investigate on the possible large central galactic density enhancement as predicted by the Navarro et al. profile, which could dramatically increase the supersymmetric dark matter discovery potential of these telescopes.

## 5 Conclusions

The results for the  $Z\gamma$  process show many similarities with the corresponding  $2\gamma$  results. For heavy neutralinos, the two lines would not be resolved so the line strengths would add. For neutralino masses below a few hundred GeV, two distinct gamma lines could be detected permitting a “spectroscopy” which could give valuable information on the nature (mass and composition) of the dark matter particles. The analytical formulas given here should be of great help to extract this information, if these gamma lines are detected.

Future gamma ray detectors may be sensitive enough to discover supersymmetric dark matter for favourable values of supersymmetric and halo parameters, although the uncertainty of the latter may make exclusion of dark matter models from the non-observation of a signal difficult.

## 6 Acknowledgements

We thank J. Edsjö and P. Gondolo for collaboration on the numerical supersymmetry calculations, and C. Frenk for useful information on halo models. The work of L.B. was supported by the Swedish Natural Science Research Council (NFR).

## Appendix A

In this Appendix, we define the functions needed to give the expression for the cross section. We start by defining the auxiliary functions

$$slog(r_1, r_2, r_3; x) \equiv \log \left[ -r_1 x^2 + (r_1 + r_2 - r_3) x + r_3 \right]\tag{A.1}$$

and

$$flog(r_1, r_2, r_3, r_4, r_5; x) \equiv \frac{1}{x - [(r_3 + r_4)/2 - r_2 - r_5]/(r_1 + r_5)} \cdot \left\{ \log \left[ \left| -r_1 x^2 + (r_1 - r_2 + r_3)x + r_2 \right| \right] - \log \left[ \left| r_5 x^2 + 1/2(r_3 - r_4)x + 1/2(r_3 + r_4) - r_5 \right| \right] \right\}. \quad (\text{A.2})$$

These enter the following integrals, which cannot be performed analytically in terms of elementary functions. We have chosen the integral expressions rather than rewriting everything in terms of dilogarithms, because the expressions are more compact and possible to integrate directly numerically.

$$I_1^4(r_1, r_2, r_3, r_4) = \int_0^1 \frac{dx}{x} [slog(-4r_1, r_2, r_3; x) - slog(-4r_4, r_2, r_3; x)] \quad (\text{A.3})$$

$$I_1^3(r_1, r_2, r_3) = I_1^4(r_1, r_2, r_2, r_3) \quad (\text{A.4})$$

$$I_1^2(r_1, r_2) = I_1^4(r_1, r_2, r_2, 0) \equiv I_1(r_1, r_2) \quad (\text{A.5})$$

$$I_2^4(r_1, r_2, r_3, r_4) = \int_0^1 \frac{dx}{x} [slog(r_1 - 2r_4, r_2, r_3; x) - slog(-r_1, r_2, r_3; x)] \quad (\text{A.6})$$

$$I_2^3(r_1, r_2, r_3) = I_2^4(r_1, r_2, 1, r_3) \quad (\text{A.7})$$

$$I_2^2(r_1, r_2) = I_2^4(r_1, r_2, 1, 0) \equiv I_2(r_1, r_2) \quad (\text{A.8})$$

$$I_3^4(r_1, r_2, r_3, r_4) = \int_0^1 \frac{dx}{x} [slog(r_1 - 2r_4, r_3, r_2; x) - slog(-r_1, r_3, r_2; x)] \quad (\text{A.9})$$

$$I_3^3(r_1, r_2, r_3) = I_3^4(r_1, r_2, 1, r_3) \quad (\text{A.10})$$

$$I_3^2(r_1, r_2) = I_3^4(r_1, r_2, 1, 0) \equiv I_3(r_1, r_2). \quad (\text{A.11})$$

$I_1(r_1, r_2)$ ,  $I_2(r_1, r_2)$  and  $I_3(r_1, r_2)$  are the functions defined in Appendix A in Ref.[2]. The notation here and in the following has been chosen such that when  $M_Z \rightarrow 0$ , the integrals have a simple relation to the ones in [2]. For example, the  $\tilde{I}^5$  function below also reduces to  $I_2$  or  $I_3$  in the appropriate limits.

$$\tilde{I}^5(r_1, r_2, r_3, r_4, r_5) = \int_0^1 dx [flog(r_1 - 2r_5, r_2, r_3, r_4, r_5; x) - flog(-r_1, r_2, r_4, r_3, r_5; x)] \quad (\text{A.12})$$

$$\tilde{I}_{2;1}^4(r_1, r_2, r_3, r_4) = \tilde{I}^5(r_1, r_2, r_3, 1, r_4) \quad (\text{A.13})$$

$$\tilde{I}_{2;2}^4(r_1, r_2, r_3, r_4) = \tilde{I}^5(r_1, r_2, 1, r_3, r_4) \quad (\text{A.14})$$

$$\tilde{I}_2^3(r_1, r_2, r_3) = \tilde{I}^5(r_1, r_2, 1, 1, r_3) \quad (\text{A.15})$$

$$\tilde{I}_3^3(r_1, r_2, r_3) = \tilde{I}^5(r_1, 1, r_2, r_2, r_3) \quad (\text{A.16})$$

For the pieces that can be integrated analytically, it is convenient to introduce the function

$$K(r, \Delta) = \begin{cases} \frac{\sqrt{\Delta}}{2} \ln \left( \left| \frac{1+(r/\sqrt{\Delta})}{1-(r/\sqrt{\Delta})} \right| \right) & \text{if } \Delta \geq 0 \\ \sqrt{-\Delta} \arctan \left( \frac{r}{\sqrt{-\Delta}} \right) & \text{if } \Delta \leq 0 \end{cases} \quad (\text{A.17})$$

$$\begin{aligned} I_4^1(a, b, c) &= \frac{1}{a-c/4} \left[ K(1+a-b-c/2, \tilde{\Delta}_1) - K(1-a-b+c/2, \tilde{\Delta}_1) \right. \\ &\quad - K(1+a-b, \Delta_2) + K(1-a-b, \Delta_2) \\ &\quad \left. + K(c, c(c-4b)) + (1-b+c/4) \log b \right] \end{aligned} \quad (\text{A.18})$$

$$\begin{aligned} I_4^2(a, b, d, c) &= \frac{1}{2(a-c/4)} \left[ K(1+a-b-c/2, \tilde{\Delta}_1) + K(d+a-b-c/2, \hat{\Delta}_1) \right. \\ &\quad - K(1-a-b+c/2, \tilde{\Delta}_1) - K(d-a-b+c/2, \hat{\Delta}_1) \\ &\quad - K(1+a-b, \Delta_2) - K(d+a-b, \hat{\Delta}_2) + K(1-a-b, \Delta_2) \\ &\quad + K(d-a-b, \hat{\Delta}_2) + K(c+1-d, \Delta_3) + K(c-1+d, \Delta_3) \\ &\quad \left. + (1/2 + d/2 - b - c/4) (2 \log b - \log d) \right] \end{aligned} \quad (\text{A.19})$$

where we have defined

$$\begin{aligned} \tilde{\Delta}_1 &= (a-c/2+b-1)^2 + 4(a-c/2) \\ \hat{\Delta}_1 &= (a-c/2+b-d)^2 + 4(a-c/2)d \\ \Delta_2 &= (b-a-1)^2 - 4a \\ \hat{\Delta}_2 &= (b-a-d)^2 - 4ad \\ \Delta_3 &= (1+d-c)^2 - 4d \end{aligned} \quad (\text{A.20})$$

Finally, for the imaginary parts we need the following functions:

$$J_1(a, b) = \log \left( \frac{1 + \sqrt{1-b/a}}{1 - \sqrt{1-b/a}} \right) \quad (\text{A.21})$$

$$J_2(b, c) = \log \left( \frac{1 + \sqrt{1-4b/c}}{1 - \sqrt{1-4b/c}} \right) \quad (\text{A.22})$$

$$J_3(a, b, c) = \log \left( \frac{1 - b + c/4 + (a - c/4) \sqrt{1 - 4b/c}}{1 - b + c/4 - (a - c/4) \sqrt{1 - 4b/c}} \right) \quad (\text{A.23})$$

## References

- [1] G. Jungman, M. Kamionkowski and K. Griest, Phys. Rep. **267** (1996) 195.
- [2] L. Bergström and P. Ullio, hep-ph/9706232.
- [3] S.C. Strausz, Phys. Rev. **D55** (1997) 4566.
- [4] L. Bergström and J. Kaplan, Astropart. Phys. **2** (1994) 261.
- [5] M. Srednicki, S. Theisen and J. Silk, Phys. Rev. Lett. **56** (1986) 263.
- [6] L. Bergström and H. Snellman, Phys. Rev. **D37** (1988) 3737.
- [7] J.H. Kühn, J. Kaplan and O. Safiani, Nucl. Phys. **B157** (1979) 125.
- [8] K. Fujikawa, Phys. Rev. **D7** (1973) 393.
- [9] J. Edsjö, Aspects of Neutrino Detection of Neutralino Dark Matter (Uppsala University thesis, Uppsala, 1997), hep-ph/9704384.
- [10] C. Itzykson and J.B. Zuber, Quantum Field Theory (McGraw-Hill, Singapore, 1980).
- [11] J. Edsjö and P. Gondolo, hep-ph/9704361 (1997).
- [12] W. Dehnen and J. Binney, astro-ph/9612059 (1997).
- [13] A. V. Kravtsov et al., astro-ph/9708176 (1997).
- [14] J.F. Navarro, C.S. Frenk and S.D.M. White, Astrophys. J. **462** (1996) 563.
- [15] V.S. Berezinsky, A.V. Gurevich and K.P. Zybin, Phys. Lett. **B294** (1992) 221.
- [16] R.A. Flores and J.R. Primack, Astrophys. J. **427** (1994) L1.
- [17] A. Burkert and J. Silk, astro-ph/9707343 (1997).
- [18] C. Frenk, private communication.
- [19] M.S. Turner, Phys. Rev. **D34** (1986) 1921.



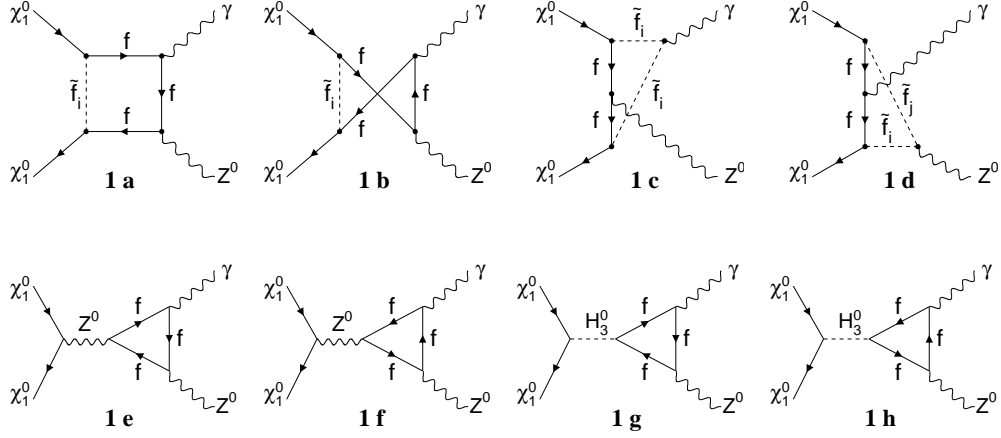


Figure 1: Feynman diagrams included in the computation of  $\tilde{\mathcal{A}}_{f\bar{f}}$ . Diagrams with exchanged initial states are not shown.

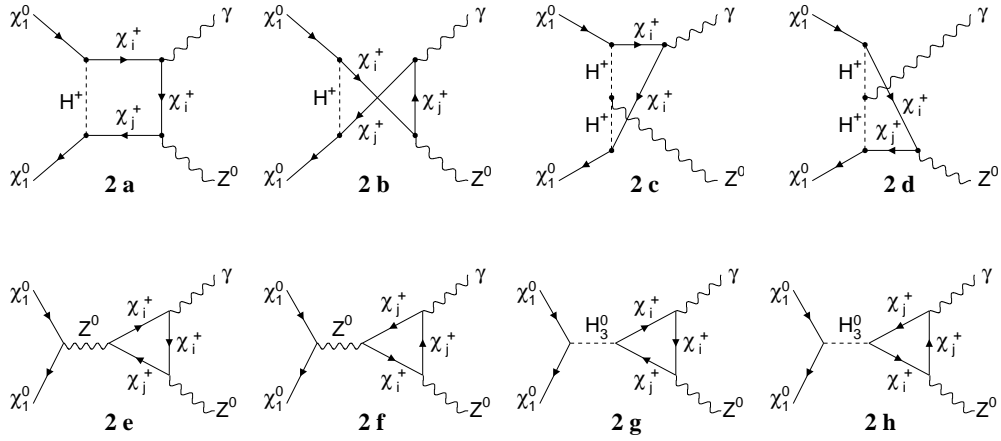


Figure 2: Feynman diagrams included in the computation of  $\tilde{\mathcal{A}}_{H^+}$ . Diagrams with exchanged initial states are not shown.

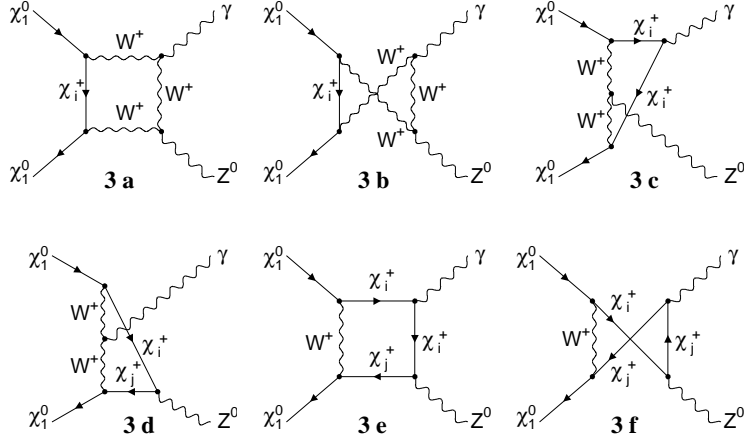


Figure 3: Feynman diagrams included in the computation of  $\tilde{\mathcal{A}}_W$ . Diagrams with exchanged initial states are not shown.

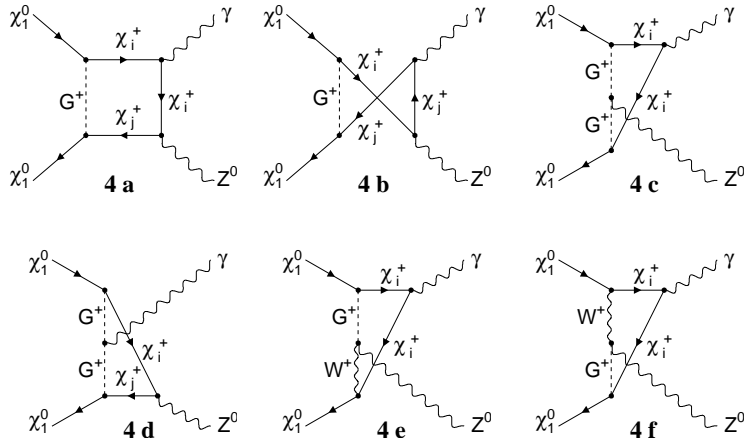


Figure 4: Feynman diagrams included in the computation of  $\tilde{\mathcal{A}}_G$ . Diagrams with exchanged initial states are not shown.

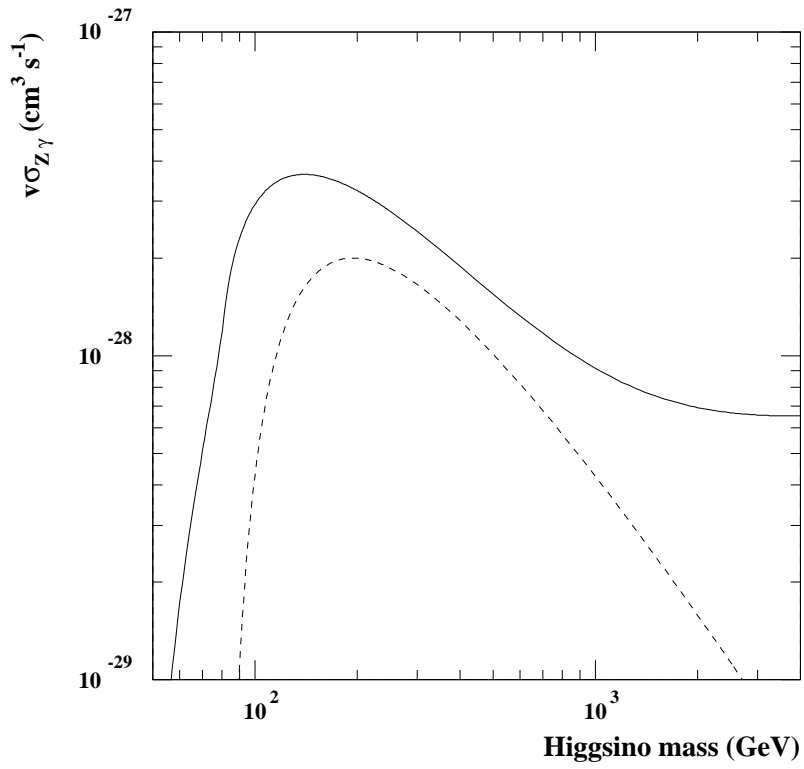


Figure 5: Annihilation rate of pure higgsinos into a photon and a  $Z^0$  boson obtained in this work (solid line). Also shown is the unitary bound coming from keeping the imaginary part only, which agrees with the result of Ref. [4] (dashed line).

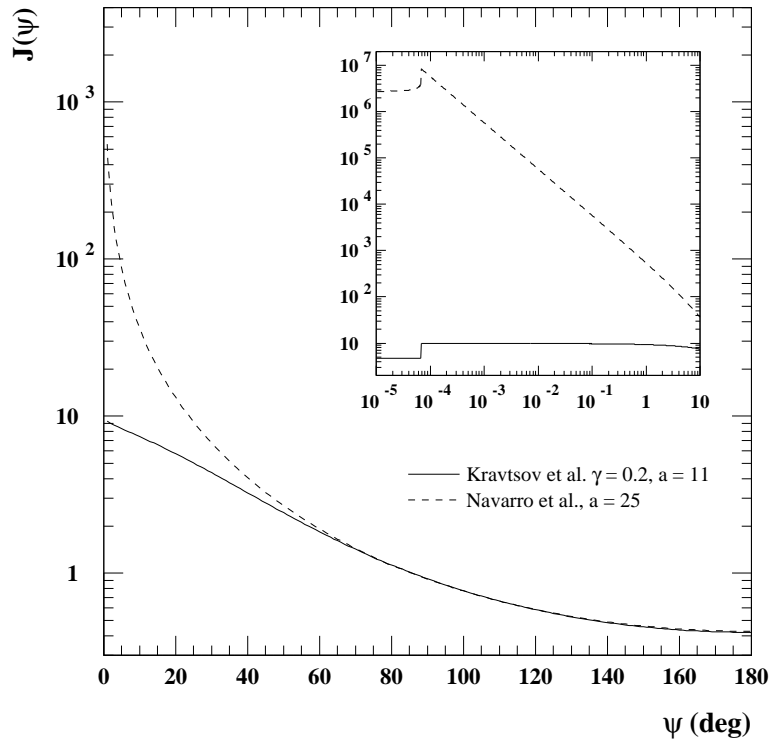


Figure 6: Function  $J(\psi)$  as defined in Eq. (18). In the detail the discontinuity in the two curves is due to the portion of halo which is hidden by the black hole at the galactic centre.